Clinical Cancer Research

Positron Emission Tomography Imaging with ^{18}F-Labeled $Z_{HER2:2891}$ Affibody for Detection of HER2 Expression and Pharmacodynamic Response to HER2-Modulating Therapies

Sebastian Trousil[1], Susan Hoppmann[2], Quang-Dé Nguyen[1], Maciej Kaliszczak[1], Giampaolo Tomasi[1], Peter Iveson[2], Duncan Hiscock[2], and Eric O. Aboagye[1]

Abstract

Purpose: Expression of HER2 has profound implications on treatment strategies in various types of cancer. We investigated the specificity of radiolabeled HER2-targeting $Z_{HER2:2891}$ Affibody, [^{18}F]GE-226, for positron emission tomography (PET) imaging.

Experimental Design: Intrinsic cellular [^{18}F]GE-226 uptake and tumor-specific tracer binding were assessed in cells and xenografts with and without drug treatment. Specificity was further determined by comparing tumor localization of a fluorescently labeled analogue with DAKO HercepTest.

Results: [^{18}F]GE-226 uptake was 11- to 67-fold higher in 10 HER2-positive versus HER2-negative cell lines *in vitro* independent of lineage. Uptake in HER2-positive xenografts was rapid with net irreversible binding kinetics making possible the distinction of HER2-negative [MCF7 and MCF7-p95HER2: NUV_{60} (%ID/mL) 6.1 $\pm$ 0.7; K_i (mL/cm^3/min) 0.0069 $\pm$ 0.0014] from HER2-positive tumors (NUV_{60} and K_i: MCF7-HER2, 10.9 $\pm$ 1.5 and 0.015 $\pm$ 0.0035; MDA-MB-361, 18.2 $\pm$ 3.4 and 0.025 $\pm$ 0.0052; SKOV-3, 18.7 $\pm$ 2.4 and 0.036 $\pm$ 0.0065) within 1 hour. Tumor uptake correlated with HER2 expression determined by ELISA ($r^2 = 0.78$), and a fluorophore-labeled tracer analogue colocalized with HER2 expression. Tracer uptake was not influenced by short-term or continuous treatment with trastuzumab in keeping with differential epitope binding, but reflected HER2 degradation by short-term NVP-AUY922 treatment in SKOV-3 xenografts (NUV_{60}: 13.5 $\pm$ 2.1 %ID/mL vs. 9.0 $\pm$ 0.9 %ID/mL for vehicle or drug, respectively).

Conclusions: [^{18}F]GE-226 binds with high specificity to HER2 independent of cell lineage. The tracer has potential utility for HER2 detection, irrespective of prior trastuzumab treatment, and to discern HSP90 inhibitor-mediated HER2 degradation. *Clin Cancer Res; 20(6); 1632–43. ©2014 AACR.*

Introduction

HER2 (also referred to as HER2/neu or ErbB-2) is a 185 kDa transmembrane receptor belonging to the epidermal growth factor receptor (EGFR) family (1). HER2 gene amplification and protein overexpression play pivotal roles in the pathogenesis and progression of many types of cancer. HER2 is overexpressed in around 20% of breast, 15% to 35% of gastric, and 9% to 32% of ovarian cancers and is correlated with poor survival (2–4). The protein has consequently emerged in recent years as an important predictive biomarker and target of cancer therapy (5). Homo- or heterodimerization with other members of its family prompts activation of the intracellular tyrosine kinase domain and triggers cell survival and proliferation mediated through MAPK and Akt signaling pathways (6, 7).

Available HER2-targeted therapies in the clinic include antibodies, such as trastuzumab (Herceptin, Genentech) and pertuzumab (Perjeta, Genentech), which prevent receptor dimerization, antibody-drug conjugates, such as T-DM1 (Kadcyla, Genentech) or small molecule inhibitors targeting the tyrosine-kinase domain (e.g., lapatinib, Tyverb, GlaxoSmithKline; a dual HER2 and EGFR inhibitor). Proteolytic shedding of the extracellular domain or alternative splicing in limited cases can generate a truncated, signaling remnant p95HER2 domain, which presents one potential mechanism of resistance to anti-HER2 therapies (8). Although trastuzumab forms the mainstay of anti-HER2-targeted therapies, it does not reverse HER2 protein expression in patients (9, 10). Inhibitors of the molecular chaperone HSP90, which elicit HER2 proteasomal degradation, are therefore currently under investigation in this context. A phase II clinical trial of one such inhibitor, NVP-AUY922

Authors' Affiliations: [1]Comprehensive Cancer Imaging Centre at Imperial College, Faculty of Medicine, Imperial College London, London; and [2]GE Healthcare, Medical Diagnostics, The Grove Centre, White Lion Road, Amersham, Buckinghamshire, United Kingdom

Note: Supplementary data for this article are available at Clinical Cancer Research Online (http://clincancerres.aacrjournals.org/).

Corresponding Author: Eric O. Aboagye, Comprehensive Cancer Imaging Centre, Faculty of Medicine, Imperial College London, Room GN1, Commonwealth Building, Hammersmith Hospital, Du Cane Road, London W12 0NN, UK. Phone: 44-208-383-3759; Fax: 44-208-383-1783; E-mail: eric.aboagye@imperial.ac.uk

doi: 10.1158/1078-0432.CCR-13-2421

Translational Relevance

Accurate assessment of a cancer patient's HER2 status remains a clinical challenge with up to 20% of patients being potentially withdrawn from therapy or exposed to unnecessary toxicity. Noninvasive imaging is widely seen as a viable alternative to current methods, in particular within the setting of locoregional and distant recurrences not amenable to biopsy, but clinical success by positron emission tomography has so far been hampered by prolonged tracer retention in liver and kidneys obstructing detection on proximate metastases. We developed a next-generation Affibody-based radiotracer, [^{18}F]GE-226, with improved properties for large-scale and good manufacturing practice–grade synthesis and enhanced pharmacokinetic characteristics. We were able to differentiate HER2 negative from low-, medium-, and high-expressing tumors by imaging and irrespective of trastuzumab pretreatment. Lineage independence of these results extends application beyond breast cancer. Because of the specific annotation to HER2 and enhanced pharmacokinetic properties, [^{18}F]GE-226 is now transitioning into clinical development.

(Novartis), has recently been completed in patients with HER2 or ER positive locally advanced or metastatic breast cancer (NCT00526045).

Accurate testing of HER2 status is crucial for patient stratification to identify individuals that may benefit most from such targeted therapies, notably trastuzumab or pertuzumab. However, this can be intricate as HER2 expression may vary through progression from primary to secondary disease with locoregional and distant recurrences often not being amenable to biopsy (11). Furthermore, recent studies have highlighted spatial heterogeneity as a potential source of incorrect assessment (12). The vast majority of U.S. Food and Drug Administration (FDA)-approved diagnostics are based on immunohistochemistry (IHC) and FISH. IHC determines the HER2 protein expression in formalin-fixed paraffin embedded tumor biopsies, whereas FISH detects HER2 gene amplifications, which are considered a legitimate surrogate as HER2 overexpression is generally caused by copy number variations (13). The utility of serum-based alternatives by detecting soluble extracellular domains is also under investigation (14).

Tumor marker–targeted molecular imaging using radiolabeled Affibodies, which are non-immunoglobulin-derived affinity proteins, might provide an accurate and noninvasive alternative to HER2 molecular diagnostics. Affibodies are engineered as 3-helix bundle Z proteins derived from the staphylococcal protein A (15). They are characterized by nano- to picomolar binding affinities, small size of ~6.5 kDa compared with antibodies or antibody fragments (~20–150 kDa), and short plasma residence time, thus permitting rapid and homogenous tissue distribution. Consequently, high-contrast images can be obtained within the first hour or 2 of administration (16, 17). Because of their favorable pharmacokinetic properties, these molecules are suitable for radiolabeling with short-lived radioisotopes by comparison with full immunoglobulin G (IgG) antibodies.

In this study, we demonstrate that the HER2-targeting Affibody [^{18}F]GE-226 provides a viable strategy to determine differential HER2 expression irrespective of lineage or pretreatment with trastuzumab within 1 hour after injection. We provide insights into the kinetic characteristics of the Affibody interaction with HER2 using full length versus p95HER2 transfected cells and siRNA HER2 as controls, or HSP90 inhibitor treatment to degrade HER2.

Materials and Methods

Chemistry and radiochemistry

[^{18}F]GE-226 was labeled using a fluorobenzaldehyde strategy optimized for automated manufacture on FASTlab, as outlined in Supplementary Fig. S1 and described elsewhere (18). Typical nondecay corrected end of synthesis yields were 30% and a radiochemical purity of 95%. The specific activity across all preparations was 38 to 110 GBq/μmol with a median of 46.2 GBq/μmol.

Cells and treatments

MCF7-vector (piRES), MCF7-p95HER2, and MCF7-HER2 cells were a kind gift of José Baselga's laboratory (19). MCF7 clones, MDA-MB-231 [American Type Culture Collection (ATCC)], MDA-MB-361 (Sigma-Aldrich), SKBR-3 (ATCC), and SKOV-3 (Sigma-Aldrich) cells were maintained in Dulbecco's Modified Eagle Medium. AGS (Sigma-Aldrich), HGC-27 (Sigma-Aldrich), NCI-N87 (ATCC), and OE-33 (ATCC) cells were maintained in RPMI (Sigma-Aldrich). A431 cells (Sigma-Aldrich) were maintained in MEM Eagle medium (Sigma-Aldrich). Growth media were supplemented with 10% FCS (Lonza), glutamine, and antibiotics (both Invitrogen). A431 cells were additionally supplemented with 1% nonessential amino acids. Cells were cultured at 37°C in humidified atmosphere containing 5% CO_2. Cell lines were authenticated by provider by short-tandem repeat analysis. No additional authentication of cells was done by the authors.

For siRNA-mediated HER2 knockdown, SKOV-3 cells were transfected with 25 nmol/L scramble control (Dharmacon, ON-TARGETplus Non-targeting Pool, Cat. No.: D-001810-10-05) or HER2-targeting siRNA (Invitrogen, ERBB2 Silencer Select Validated siRNA; Cat. No.: 4457298) by reverse transfection with Lipofectamine RNAiMAX (Invitrogen) according to manufacturer's instructions. A total of 3×10^5 cells were seeded in 12-well plates 48 hours before uptake experiment. Target knockdown was verified by Western blotting on cells that were transfected in parallel.

For all uptake studies in response to drug treatment, 2.5×10^5 SKOV-3 cells were seeded in complete medium 48 hours before uptake experiments. Cells were incubated with indicated doses of NVP-AUY922 (LC Laboratories) for

24 hours and 10 μg/mL trastuzumab (Roche) for 1 or 24 hours before addition of radiotracer.

In vitro uptake assay

For baseline uptake, 3×10^5 cells were seeded in complete media in 12-well plates (Corning) and allowed to recover overnight. Cells were washed twice with serum-free medium and pulsed with 370 kBq in 500 μL serum-free medium for 1 hour. For blocking studies, cells were co-incubated with tracer and 0.5 mg/mL cold, isotopically unmodified GE-226.

Cells were washed with PBS, trypsinized, neutralized with complete medium, and centrifuged. The pellet was washed 3 times with PBS and lysed in 120 μL radioimmunoprecipitation assay buffer (Sigma-Aldrich). The radioactivity of 100 μL lysate was counted on a Packard Cobra II gamma counter (Perkin Elmer). Radioactivity was normalized to applied radioactivity and protein content, as determined by bicinchoninic acid assay (Pierce).

Small animal experimental models for PET

All animal experiments were conducted by licensed investigators in accordance with the United Kingdom Home Office Guidance on the Operation of The Animals (Scientific Procedures) Act 1986 Amendment Regulations 2012 and within the published guidelines for the welfare and use of animals in cancer research (20). The *in vivo* experimental models were established in female BALB/c nude mice ages 6 to 8 weeks (Harlan). For all but SKOV-3 xenografts, mice were subcutaneously implanted with 0.72 mg/60 day release estradiol pellets (Innovative Research of America, Sarasota, FL) approximately 2 days before cell inoculation. Xenografts were established by subcutaneously injection of 100 μL MCF7-vector, MCF7-p95HER2 and MCF7-HER2 cells (1.5×10^7 cells in PBS mixed 1:1 with Matrigel, BD Biosciences), MDA-MB-361 cells (5×10^6 cells in PBS mixed 1:1 with Matrigel), or SKOV-3 cells (5×10^6 cells in PBS) on the back of mice. Tumor dimensions were measured frequently by caliper measurements and volumes calculated by the following equation: volume $mm^3 = (\pi/6) \times a \times b \times c$, where a, b, and c represent 3 orthogonal axes of the tumor. When tumor volumes reached approximately 50 to 100 mm^3 (MCF7 models ~4 weeks postinjection, MDA-MB-361 xenografts ~3 weeks postinjection, and SKOV-3 xenografts ~6 weeks postinjection), mice were used for biodistribution or PET imaging studies.

For blocking studies, SKOV-3 xenograft bearing mice were administered 500 μg (~25 mg/kg) cold isotopically unmodified GE-226 intravenously through the tail vain 20 minutes before administration of radiotracer. To assess interaction of radiotracer with trastuzumab, SKOV-3 xenograft-bearing mice were treated with 50 mg/kg trastuzumab intraperitoneally 2 hours before the scan. Animals were recovered, treated twice more with 25 mg/kg trastuzumab intraperitoneally and re-scanned 7 days after initial dose. To investigate response to HSP90 inhibition, SKOV-3 xenograft-bearing mice were treated with 50 mg/kg NVP-AUY922 or equivalent volume of vehicle (~5 μL/g body weight; 10% dimethyl sulfoxide and 5% Tween-20 in PBS) every day intraperitoneally for 3 days. Twenty-four hours after the last treatment, animals were used for PET imaging.

PET-computed tomography imaging

Mice were anesthetized through isoflurane inhalation and scanned on a small animal PET-computed tomography (PET-CT) scanner (Siemens Multimodality Inveon). Low-dose CT scans were first acquired (80 kVp, 0.5 mA, 220° rotation, 600 ms per degree exposure time, 80 μm reconstruction pixel size) for PET attenuation correction and anatomical reference. PET images were acquired following a bolus intravenous injection of approximately 3.7 MBq [^{18}F]GE-226 in the tail vein. Dynamic emission scans were acquired in list mode format over 60 minutes. Data were sorted into 0.5-mm sinogram bins and 19 time frames for image reconstruction by filtered back projection (4×15 seconds, 4×60 seconds, and 11×300 seconds). The Siemens Inveon Research Workplace software was used for visualization of radiotracer uptake. Thirty- to sixty-minute cumulative images of the dynamic data were used to define 3-dimensional regions of interest (ROI). Arterial input function was estimated by drawing ROIs over the center of the heart cavity using cumulative images from 0.25 to 2 minutes of the dynamic series, a method, we previously validated for use in rodents (21). The count densities were averaged for all ROIs at each time point to obtain time versus radioactivity curves (TAC). Tumor TACs were normalized to injected dose measured by a VDC-304 dose calibrator (Veenstra Instruments) and normalized uptake was expressed as percentage injected dose per mL tissue (NUV; %ID/mL). Normalized uptake of radiotracer at 60 minutes (NUV_{60}) was used for comparisons. For qualitative image visualization, cumulative images of the dynamic data (30–60 minutes) were also iteratively reconstructed (OSEM3D).

Kinetic modeling

Kinetic analysis of PET data was performed applying a standard 2-tissue irreversible compartmental model to fit each tumor TAC with the corresponding image-derived plasma TAC as input function (IF) to estimate K_1 (mL/cm^3/min), k_2 (1/min), and k_3 (1/min) and the blood vascular component V_b (mL blood/mL tissue; unitless). The irreversible uptake rate K_i (mL/cm^3/min) was computed as $K_1 \times k_3/(k_2 + k_3)$. To estimate the kinetic parameters the measured tumor TAC (tTAC) was modeled as

$$tTAC(t) = (1 - V_b)h(t) \otimes pIF(t) + V_b IF(t)$$

with $h(t)$ indicating the unknown tissue impulse response function and $\otimes$ the convolution operator. The parameter vector $p = [K_1, k_2, k_3, V_b]$ was estimated with the standard weighted non-linear least squares (WNLLS) by minimizing the weighted residual sum of squares (WRSS) function

$$WRSS(p) = \sum_{i=1}^{N} w_i \left[tTAC(t_i, p)^{MODEL} - tTAC(t_i) \right]^2$$

with $tTAC(t_i)$ and t_i indicating the measured concentration in the tumor and mid-time of ith frame, respectively, and N denoting numbers of frames. Weights w_i were set to

$$\frac{\Delta_i}{C(t_i)\exp(\lambda t_i)}$$

with Δ_i and λ representing the duration of the ith frame and decay constant of ^{18}F (22). The 2-tissue irreversible model was chosen after visual assessment of the tumor TACs, which showed clear irreversible uptake in most cases. Furthermore, when a 2-tissue reversible compartment model was used, nonphysiologic estimates of the parameters characterized by high variance were obtained.

Statistical analysis

Data were expressed as mean ± SD or SEM. Unless otherwise specified, the significance of comparison between 2 datasets was determined using unpaired, 2-tailed Student t test (GraphPad Prism version 5.1) and $P < 0.05$ defined as significant.

The Supplementary Information contains further experimental procedures, including synthesis of fluorescein labeled GE-226, surface plasmon resonance, Western blotting, biodistribution, metabolic stability, small animal models for fluorescent GE-226 experiments, IHC, ELISA, and sequencing.

Results

Affibody-HER2 binding properties

To ensure the fluorinated prosthetic group does not adversely influence the Affibody binding kinetics, we measured the receptor interaction of the isotopically unmodified Affibody analogue using surface plasmon resonance and compared this to binding of human full-length and truncated p95HER2, as well as rhesus and rat full-length HER2. Although the tracer showed very strong binding to human (K_D = 76 pmol/L) and rhesus HER2 (K_D = 67 pmol/L), it did not interact with p95HER2 or rat HER2 (Table 1 and Supplementary Fig. S2).

Table 1. Summary of binding kinetics of GE-226 to human and rhesus HER2

Kinetic properties	Human HER2	Rhesus HER2
On-rate k_{on}	1.73×10^7 per mol/L per second	6.37×10^6 per mol/L per second
Off-rate k_{off}	1.31×10^{-3} per second	4.25×10^{-4} per second
Affinity K_D	7.58×10^{-11} mol/L	6.67×10^{-11} mol/L
R_{max}	133.5	138.1
χ^2	0.607	1.12
U-value	3	7

[^{18}F]GE-226 exhibits specific and lineage-independent HER2 binding

We tested the tracer retention in 10 different cell lines derived from breast, upper gastrointestinal tract, and ovarian cancer, of which half were HER2 negative and the other half HER2 positive. The panel included an isogenic model comprising of HER2-negative MCF7 cells, which were transfected with empty vector (MCF7-vector), p95HER2 (MCF7-p95HER2), or full-length HER2 (MCF7-HER2). Although all HER2-negative and p95HER2 transfected cell lines had only marginal background uptake (1.2% ± 0.5% applied radioactivity per mg protein across all lines), all HER2-positive cell lines retained the tracer at high levels (between 13.6% ± 3.4% and 79.9% ± 12.1% applied radioactivity per mg protein) and in good agreement with endogenous HER2 expression. Tracer binding was, however, independent of expression of another EGFR family member. Figure 1A shows one representative uptake experiment, as initial experiments revealed that the uptake was dependent on the specific activity. In comparison to freshly prepared [^{18}F]GE-226, the same radiotracer preparation yielded only 39.5% ± 8.5% and 24.9% ± 3.8% tracer uptake if incubation was initiated 70 and 140 minutes later (Supplementary Fig. S3).

To further investigate the specificity of the signal, we co-incubated SKOV-3 cells with tracer and large excess (~2,000 fold) of its nonradioactive ^{19}F-labeled analogue (Fig. 1B). This reduced uptake to 3.1% ± 2.6% compared with control cells (100% ± 12%; $P < 0.0001$). Furthermore, transient siRNA-mediated knockdown of HER2 decreased tracer uptake compared with nontargeting scramble control (Fig. 1C; 100% ± 12% vs. 18% ± 9%, $P < 0.0001$). Target knockdown was confirmed by Western blot analysis.

[^{18}F]GE-226 exhibits a different binding site than trastuzumab and predicts detection of HER2 degradation by NVP-AUY922

An important question when developing a HER2-targeting imaging probe is whether the tracer can correctly determine the HER2 status of a patient independently of potential trastuzumab treatment. Pretreatment of SKOV-3 cells with 10 μg/mL trastuzumab for 1 hour did not alter tracer binding, however, incubation for 24 hours before uptake experiment reduced tracer binding by 32% ± 11% compared with drug-naïve controls (Fig. 2A; $P < 0.0001$).

We hypothesized that HER2 degradation consequent to HSP90 inhibition (HER2 is a client protein of HSP90; ref. 23) would result in detectable changes in tracer uptake. The HSP90 inhibitor NVP-AUY922 caused a dose-dependent decrease of HER2 protein expression compared with untreated controls, which consequently translated into reduced tracer uptake, further supporting its specificity (Fig. 2B; $P < 0.0001$ for all tested concentrations compared with control).

[^{18}F]GE-226 discriminates differential HER2 expression *in vivo*

Based on the *in vitro* data, we wanted to scrutinize the ability of the tracer to distinguish varying degrees of HER2

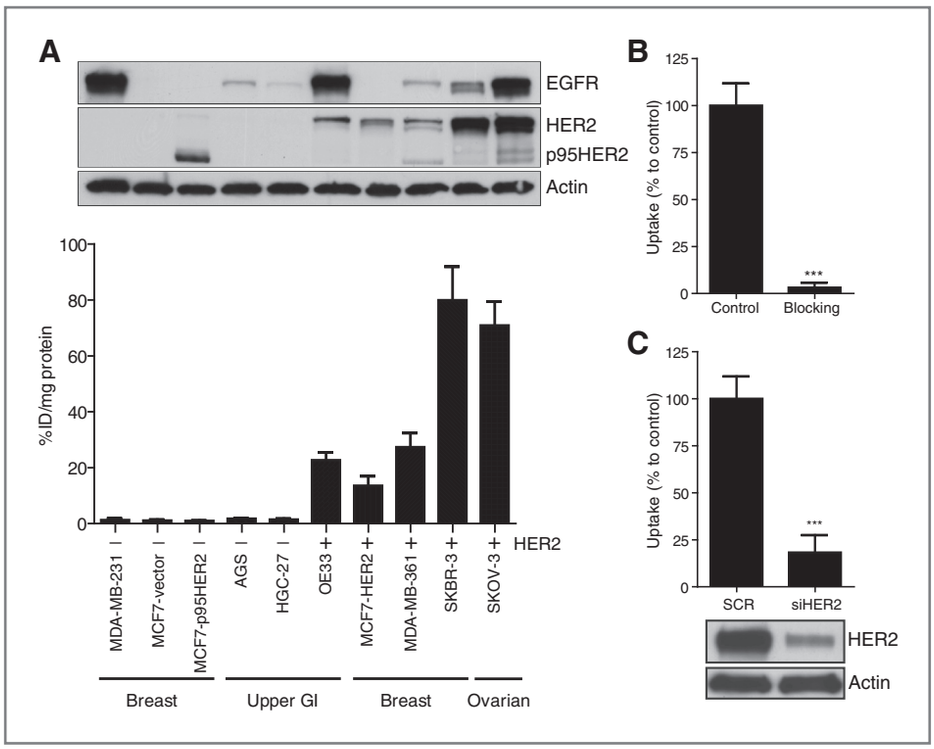

Figure 1. [^{18}F]GE-226 binds with high selectivity and sensitivity to HER2. A, cell lines of diverse lineages and differential HER2 status were exposed to [^{18}F]GE-226 for 60 minutes and retained radioactivity measured as percent applied radioactivity normalized to total protein (mean of $n = 1$ with 5–6 replicates ± SD). Full-length and truncated p95 HER2 protein expression as determined by Western blot analysis is shown for the same cell lines in the panel above. B, SKOV-3 cells were incubated with [^{18}F]GE-226 in the presence or absence of 0.5 mg/mL blocking dose of isotopically unmodified GE-226 for 60 minutes and cell-bound activity measured (***, $P < 0.0001$; mean of $n = 3$ in triplicate on 3 different days ± SD). C, HER2 expression was transiently abrogated by siRNA and tracer retention after 60 minutes compared with nontargeting scramble control (***, $P < 0.0001$; mean of $n = 3$ in triplicate on 3 different days ± SD); knockdown confirmed by Western blot analysis.

expression in the complex tumor milieu *in vivo*. Figure 3A shows representative small-animal [^{18}F]GE-226 PET images of SKOV-3 and MCF7-vector xenograft-bearing mice. High tumor uptake contrasts the low nonspecific retention in the body. The tracer was metabolically stable and predominately and rapidly excreted via the renal route (Supplementary Fig. S4 and Table S1). Across different tumor models, the tracer discriminated well between HER2-positive and HER2-negative xenografts. Both tumor-specific distribution and retention kinetics accounted for these differences. Although HER2-negative MCF7-vector and MCF7-p95HER2 xenografts exhibited low tumor retention and a steady-state tissue radioactivity after initial delivery, HER2-positive xenografts had increased uptake and followed a pattern of net irreversible binding (Fig. 3B). Thus, [^{18}F]GE-226 PET was able to distinguish HER2-negative

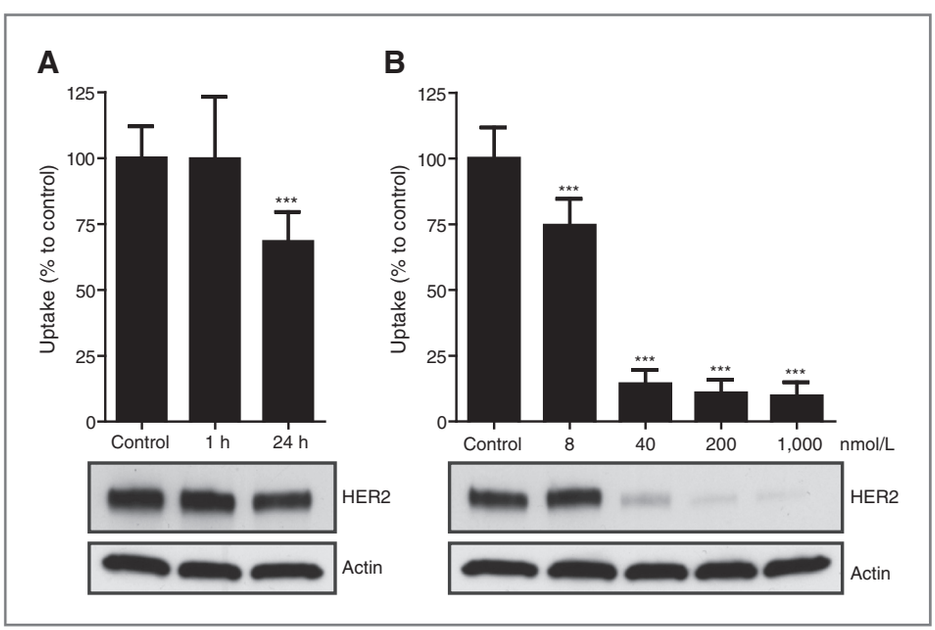

Figure 2. [^{18}F]GE-226 possesses a different binding site than trastuzumab and detects HER2 degradation upon HSP90 inhibition. A, SKOV-3 cells were treated with 10 μg/mL trastuzumab for 1 or 24 hours and incubated for an additional hour with [^{18}F]GE-226 and retained activity compared with untreated controls (***, $P < 0.0001$; mean of $n = 5$ in triplicate on 5 different days ± SD). Effect on HER2 protein expression is shown in the panel below. B, effect of HSP90 inhibitor NVP-AUY922 on HER2 expression and consequent impact on tracer uptake (***, $P < 0.001$ for all concentrations compared with control; mean of $n = 3$ in triplicate on 3 different days ± SD).

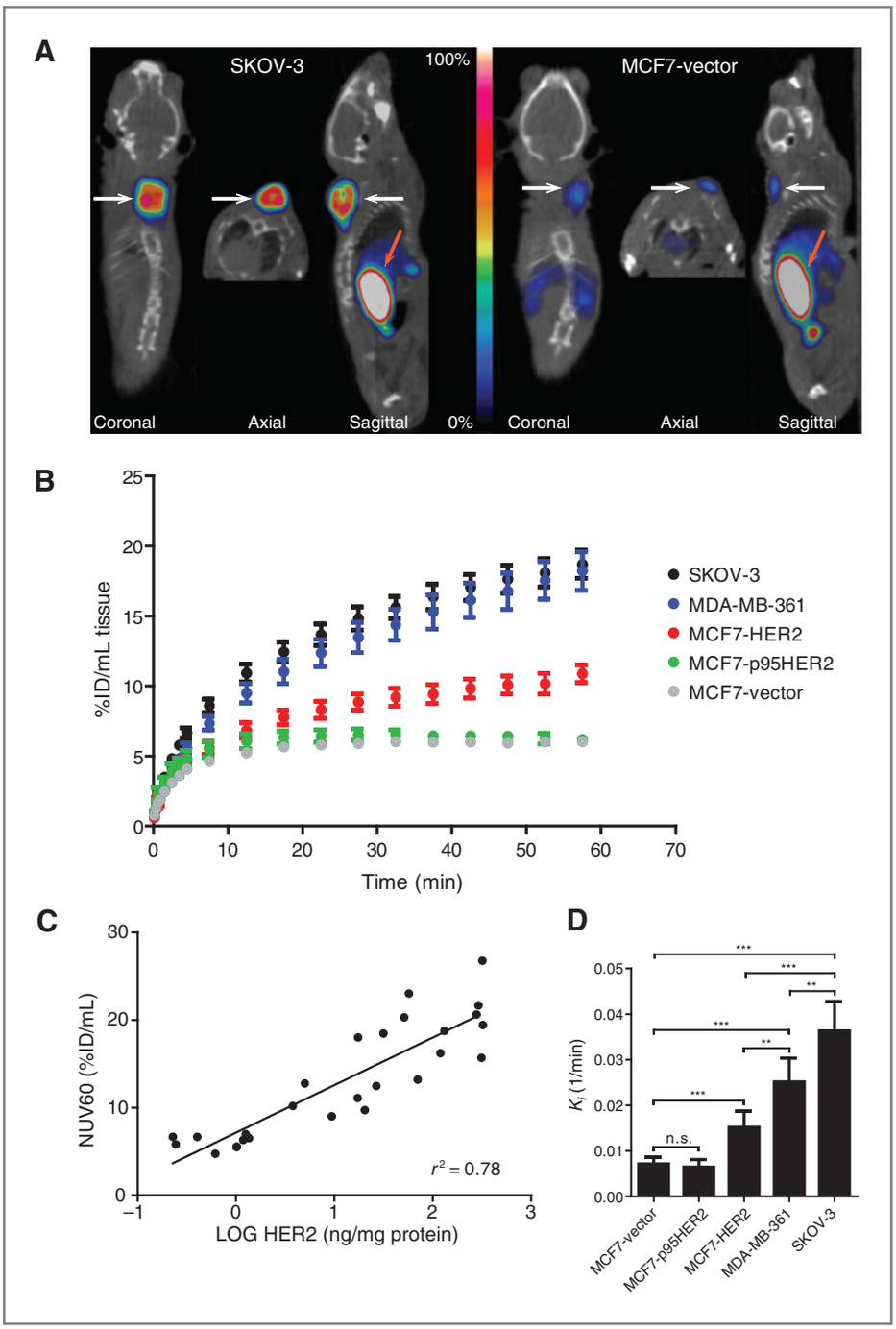

Figure 3. Tumor profiles of [^{18}F]GE-226 in differentially HER2-expressing xenograft models. A, representative OSEM3D reconstructed PET-CT images of SKOV-3 and MCF7-vector xenograft-bearing mice. White arrow indicates tumor, orange arrow kidney. B, comparison of tumor TACs in indicated xenograft models (mean of $n = 6 \pm$ SEM with exception of MCF7-p95HER2 $n = 3 \pm$ SEM). C, correlation between NUV_{60} and HER2 expression as determined by ELISA on tumor samples, that were excised postimaging. D, tissue pharmacokinetic analysis using a single input 2-tissue 3k model to derive K_i, the rate constant for the net irreversible retention of the tracer in the tumor (n.s., non-significant; **, $P < 0.01$; ***, $P < 0.001$).

(MCF7-vector and MCF7-p95HER2) from low (MCF7-HER2) and moderately (MDA-MB-361) HER2-expressing xenografts. However, tissue radioactivity was comparable in tumors with moderate and highly (SKOV-3) HER2 expression when simple measures of uptake were used for PET analysis. Nonetheless, radiotracer uptake correlated well with HER2 protein expression as determined by ELISA ($r^2 = 0.78$; Fig. 3C and Supplementary Fig. S5).

We hypothesized that kinetic modeling, which accounts for tissue uptake relative to plasma as opposed to tissue uptake alone, could further help discern the various HER2 groups. We used a 2-tissue irreversible compartmental model to derive the net irreversible uptake rate constant, K_i (Fig. 3D). No metabolite correction was necessary as the tracer was stable *in vivo* (Supplementary Fig. S4A). With this model, we could distinguish all groups, even MDA-MB-361

from SKOV-3 xenografts (Fig. 3D). As expected, K_i highly correlated with NUV_{60} among all groups ($r^2 = 0.82$; Supplementary Fig. S5D).

To lend further support to the specificity of the Affibody, we carried out blocking studies by injecting 30 mg/kg isotopically unmodified GE-226 intravenously 20 minutes before PET scan (~100-fold mass equivalent of hot tracer). The cold ligand, by blocking specific binding sites, resulted in significantly reduced tracer uptake (NUV_{60} 18.7 ± 2.4 vs. 7.1 ± 1.6 in controls and blocked tumors, $P = 0.0003$) and K_i (Supplementary Fig. S5). It is noteworthy that the kinetics of tracer uptake were distinctly different between controls and blocked samples, in that the latter share characteristics of HER2-negative tumors.

Localization and intensity of fluorescein-labeled GE-226 correlates with DAKO HercepTest

To examine tissue localization, we labeled GE-226 with fluorescein and compared localization and fluorescent intensity in tumor sections with FDA-approved DAKO HercepTest. In contrast to PET experiments, normalization to injected dose is not possible with fluorescent compounds. To eliminate intersubject variability, we performed experiments in bilateral tumor-bearing mice. Because HER2-positive and HER2-negative xenografts described in Fig. 3 have greatly varying growth rates and require differential hormonal treatments, we used A431 (HER2-negative) and NCI-N87 (HER2-positive) xenografts as previously described (18). A mixture of 20 mg/kg Hoechst and 15 mg/kg fluorescein-conjugated GE-226 in PBS were injected intravenously and 2-hour postinjection, tumors were excised, formalin fixed, and paraffin embedded and adjacent tumor sections prepared for HercepTest staining or fluorescent microscopy. Tissue processing for immunofluorescence microscopy removed any unbound tracer and signal therefore accounts only for specific HER2–Affibody interaction. Figure 4 shows that fluorescent staining colocalized with regions that are HER2 positive in NCI-N87 tumors and that both HercepTest and fluorescent staining in A431 tumors were negligible.

[^{18}F]GE-226 can correctly assess HER2 status independently of prior trastuzumab treatment and predicts for response to NVP-AUY922 *in vivo*

SKOV-3 tumor-bearing mice were treated with 3 doses of trastuzumab and imaged 2 hours post initial dose and re-imaged 48 hours after last treatment (i.e., 7 days after initial scan). Neither treatment adversely affected tumor tracer retention (Fig. 5A), albeit 7 days of continuous treatment reduced K_i by 24% ($P = 0.025$) as a consequence of elevated arterial input function and altered renal excretion (Fig. 5B and Supplementary Fig. S6). This confirmed by comparison to trastuzumab that the Affibody possesses different HER2-binding sites. Interestingly, one mouse had significantly reduced uptake on both scans and was viewed separately for analysis. We could not correlate tracer uptake with ELISA-derived HER2 expression values, as one of the ELISA antibodies interfered with bound trastuzumab. We therefore confirmed by Western blot analysis that trastuzumab treatment did not substantially alter HER2 expression nor resulted in expression of truncated P95HER2 in the outlier sample (Supplementary Fig. S7A). Sequencing exon 8 of HER2, which has been previously described as a site for mutations on the extracellular domain of HER2 (24),

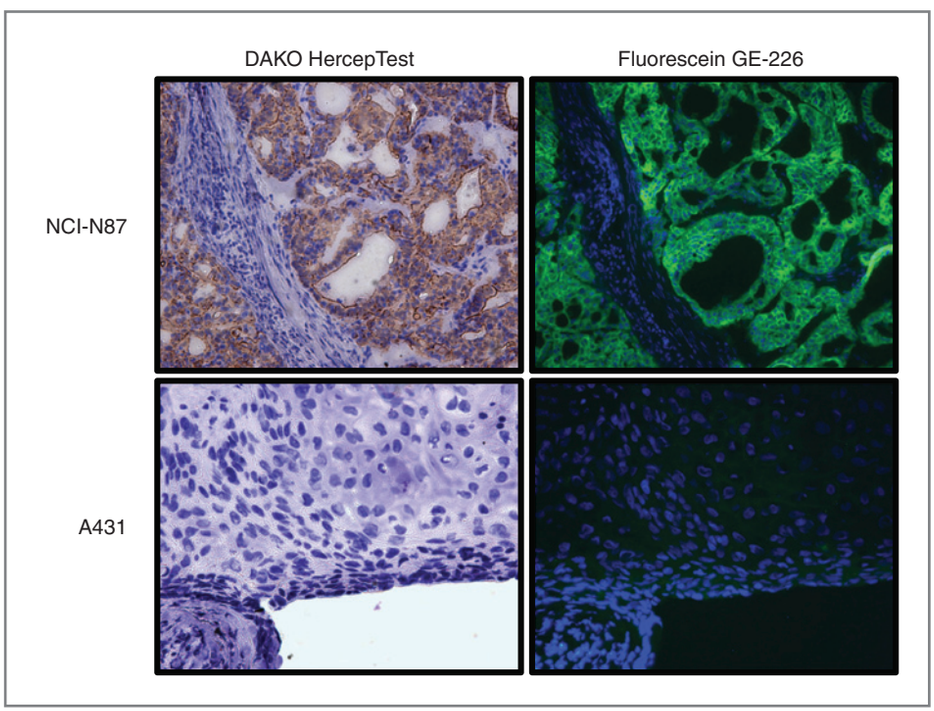

Figure 4. GE-226 colocalizes with HER2 protein expression in tumors with spatial heterogeneity. GE-226 was labeled with fluorescein and injected in mice bearing both NCI-N87 and A431 tumors, which express high and low levels of HER2, respectively. Tumors were sectioned and adjacent slides either stained with DAKO HercepTest or used for immunofluorescent microscopy.

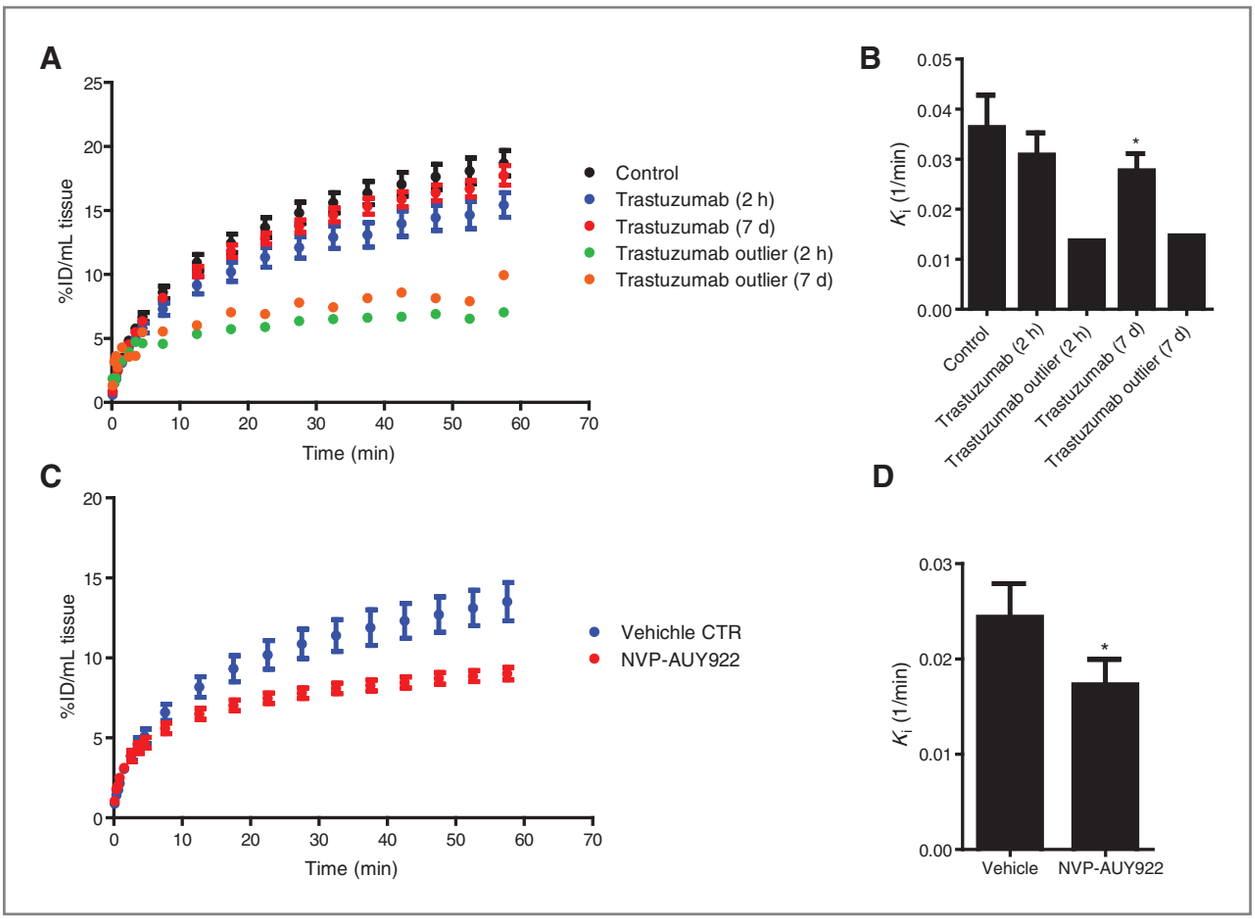

Figure 5. [^{18}F]GE-226 binding does not interfere with trastuzumab treatment and can predict response to HSP90 inhibition. A, mice bearing SKOV-3 xenografts were treated with 50 mg/kg trastuzumab intraperitoneally 2 hours before scan. Animals were recovered, treated twice more with 25 mg/kg trastuzumab, and re-imaged 7 days after initial scan ($n = 6 \pm$ SEM). One mouse, which was an outlier with low tracer uptake both on early and late scan, is displayed separately. B, pharmacokinetic analysis of A (*, $P = 0.025$). C, comparison of NVP-AUY922 treatment ($n = 5 \pm$ SEM) to vehicle-treated controls ($n = 4 \pm$ SEM) in the SKOV-3 xenograft model and (D) kinetic analysis of inhibition constants (*, $P = 0.011$).

indicated no sequence alterations in the outlier sample compared with controls (Supplementary Fig. S7B). Furthermore, kinetic modeling revealed increased tissue efflux (k_2) of the outlier with similarities to HER2-negative tumors, suggesting a loss of interaction of the Affibody with its target (Supplementary Fig. S7C–S7G). Finally, we wanted to assess whether [^{18}F]GE-226 is responsive to HSP90 inhibitor treatment *in vivo*. We treated SKOV-3 xenograft bearing mice with 3 doses of 50 mg/kg NVP-AUY922 or vehicle. This led to reduced HER2 expression with consequently decreased tracer uptake (Fig. 5C and D and Supplementary Fig. S8B).

Discussion

With aid of kinetic modeling, we demonstrate that the $Z_{HER2:2891}$ Affibody, [^{18}F]GE-226, quantitatively discriminates between HER2-negative and HER2-positive tumors within 1 hour, independent of lineage and prior treatment with trastuzumab. Affibody radiotracers have been developed to overcome the shortcomings of large (150 kDa) antibodies. To date, most of the reported studies of radiolabeled Affibodies in the literature have used analogs of $Z_{HER2:342}$ labeled with radiometals or radiohalogens (17, 25–31). Recently, re-engineering of this Affibody by Feldwisch and colleagues (32) led to an optimized scaffold containing 11 amino acid substitutions in the nonbinding surface of the Affibody removing similarity to the original protein A domain—$Z_{HER2:2891}$. Further to potential for automated site-specific good manufacturing practice-grade (33) manufacture on FASTlab to allow broad clinical access to a HER2-imaging agent, $Z_{HER2:2891}$ has improved thermal and chemical stability by avoiding deamidation, as well as increased hydrophilicity of the nonbinding surface; positive attributes for ease of peptide synthesis and *in vivo* pharmacokinetics. The latter property is desirable to permit conduct of imaging studies within 1- to 2-hours postradiotracer injection. However, within this early period, nonspecific uptake could contribute to tissue signal. We therefore assessed the specificity of ^{18}F-radiolabeled $Z_{HER2:2891}$

Affibody, [^{18}F]GE-226, for early imaging (1 hour) using both intrinsic cellular uptake and *in vivo* dynamic imaging to quantitatively discriminate between HER2-negative and HER2-positive tumors.

Optimization of contrast is pivotal to successful development of imaging agents. High contrast results largely from high affinity of radiotracers and rapid pharmacokinetics. By comparison with other molecular imaging probes, Affibodies benefit from a short blood circulation time and high target affinity resulting in high-contrast images within a relatively short time after injection, and slower internalization rates (26, 34, 35). This permits utilization of more widely available short-lived radioisotopes, such as ^{18}F and ^{68}Ga, minimizing the patient's dosimetry. In comparison with nanobodies, Affibodies excel through lower K_D, higher k_{on}, and slower k_{off} rates (36). Regarding affinity, surface plasmon resonance experiments with isotopically unmodified GE-226 revealed high affinity binding to human and rhesus HER2-ECD-Fc comparable to the binding of parent $Z_{HER2:2891}$ Affibody to human HER2-ECD-Fc (76 pmol/L; ref. 32). In contrast, GE-226 did not interact with rat HER2-ECD-Fc or human p95HER2, demonstrating specificity to the ECD-containing human protein. Radiofluoridation to produce [^{18}F]GE-226 did not affect radiotracer affinity either, as demonstrated by high-specific cell intrinsic uptake in HER2-positive versus HER2-negative human breast, upper-gastrointestinal and ovarian cancer cell lines. Notably, the lineage independence observed also lends support to the specificity of the radiotracer for HER2 versus other targets such as EGFR and potential utility in cancers other than breast.

Although preclinical imaging with $Z_{HER2:2891}$ radiolabeled with ^{111}In for single photon computed emission tomography (SPECT) displays good tumor targeting in SKOV-3 xenografts (34), it is expected that [^{18}F]GE-226 with the superior sensitivity, resolution, and quantification of PET will provide improved contrast at the early time points.

Regarding systemic tracer disposition, high renal accumulation is characteristic of radiometal tracers because of loss of the radioactive ion and reabsorption in the proximal tubules (37). In this context previous Affibodies labeled with ^{68}Ga or ^{111}In showed approximately 10-fold higher renal localization than that seen in tumor (34, 35, 38), precluding imaging of tumors in the region around the kidney, as well as having an impact on dosimetry. Bioconjugation of the Affibody molecule with albumin, histidine containing tags or ^{18}F radiolabels have been proposed as alternative approaches to avoid tubular reabsorption and permitting rapid glomerular filtration (26, 39–41). Using a radiohalogen strategy with ^{18}F, we demonstrated rapid renal clearance of [^{18}F]GE-226, without substantial tracer accumulation in the kidneys; kidney radioactivity levels were comparable to levels in tumors at 60 minutes. Uptake in other organs, including the liver, was negligible and it remains elusive whether previously detected hepatic uptake of other Affibodies in the clinical setting is attributed to Affibody disposition or the labeling strategy (42).

This suggests that [^{18}F]GE-226 could be used for detection of HER2 expression in primary tumors and distant metastasis, including liver, lung, and bone. In our study, [^{18}F]GE-226 did not cross the blood–brain barrier so its utility for imaging of brain metastases remain to be seen.

Several lines of evidence indicated that the binding of [^{18}F]GE-226 to HER2 is highly specific: (i) the tracer discriminated between HER2-positive and HER2-negative cells and tumors, (ii) siRNA knockdown of HER2 protein in cells reduced tracer uptake, (iii) pretreatment of cells or mice with isotopically unmodified GE-226 resulted in significant reduction in uptake, and (iv) tumor distribution of fluorescein-labeled GE-226 colocalized with HER2 protein as determined by DAKO HercepTest. The latter also demonstrated that tumor distribution of the Affibody was nonlimiting in the heterogeneous tumor models studied. We intimate that the above desirable affinity, specificity, and pharmacokinetic properties of [^{18}F]GE-226 led to very high-contrast PET images. We acknowledge that the high-contrast images are perhaps due also in part to the lack of tracer binding to rodent HER2 (Supplementary Fig. S2), nonetheless, it further substantiates the low nonspecific binding of [^{18}F]GE-226 as rodent data for Affibodies have been shown to translate well into human imaging profile.

We observed an influence of specific radioactivity on Affibody uptake *in vitro* where receptor numbers are limited in part due the 2D properties of *in vitro* culture, compared with a 3D system *in vivo*. We hypothesize that with the higher amount of cold compound associated with the same level of radioactivity over time, the limited specific binding sites of an *in vitro* culture system are more readily blocked and result in a time-dependent decrease of tracer uptake. As this effect was not observed *in vivo*—potentially because of a much greater overall availability of receptors—we do not anticipate this finding to hamper clinical development.

PET imaging demonstrated rapid tracer uptake in HER2-positive xenografts with net irreversible binding kinetics over time. The irreversible uptake (over the time of imaging) made it possible to distinguish between HER2-negative and HER2-positive tumors within 1 hour. TACs revealed steady-state (limited-washout) background uptake in HER2-negative xenografts, which was in keeping with the normal distribution kinetics of these types of peptides within the literature (26, 38, 43). In HER2-negative xenografts (MCF7 and MCF7 p95HER2), uptake was rapid and remained stable over the 60-minute scan period. As washout mechanisms are primarily determined by size, tissue retention of Affibodies is longer than of small molecules, nonetheless more favorable than full immunoglobulins. Thus, the uptake observed in HER2-negative tumors can be attributed to nonspecific background tissue distribution. In contrast, all HER2-positive models showed a continuous increased uptake throughout image acquisition timeframe. We confirmed that the net irreversible trapping of the tracer in tumor was not because of differences in tracer delivery (K_1) or blood volume (V_b) but rather to specific uptake. Tumor uptake correlated with HER2 expression and we attribute this to specific Affibody–HER2 interaction, and possibly

some receptor internalization (26, 34, 35). Receptor internalization was not assessed in this study but localization of the fluorescein-labeled Affibody *in vivo* did not suggest substantial internalization within the timeframe of the study. Importantly, kinetic modeling permits definition of a threshold for HER2 positivity by determining the irreversible uptake in HER2-positive tumors. This concept requires clinical evaluation, but preliminary data indicate reliable detection of HER2-positive and HER2-negative lesions. Notably, a negative scan will be a clinically determined quantitative or semiquantitative uptake cut-off value at a defined postinjection time, for example 1 hour, because of Affibody tracer distribution kinetics, and not, an absolute negative signal as seen by IHC.

In view of trastuzumab being the most important HER2-targeting therapy, we wanted to ensure that tracer and antibody did not compete for the same extracellular epitope. X-ray crystallography revealed that Z_{HER2} Affibodies bind the extracellular domain of HER2 at the interface of domains III and IV, distinct from the trastuzumab binding site on domain IV (44). We confirmed, both *in vitro* and *in vivo*, that uptake of [^{18}F]GE-226 was not obscured by the presence of trastuzumab. Minor, but significant, decreases in uptake after 24 h pretreatment with trastuzumab *in vitro* are more likely related to altered receptor internalization or other dynamics due to the high concentration used (45, 46). Continuous exposure of SKOV-3 xenografts to trastuzumab resulted in a slight downregulation of HER2 protein expression, as detected by Western blot analysis. This contrast to clinical data has been previously reported for preclinical models (27), but further validation would be required to investigate which of the complex dynamic changes upon trastuzumab treatment—including receptor internalization, changes in vascularization, immune response, cell death and selection of HER2-negative subpopulations—account for these discrepancies. In the *in vivo* studies, one HER2 tumor-bearing mouse was characterized by low tumor tracer uptake. As HER2 was found not to be truncated in this sample (Western blot analysis), mutations in the extracellular domain of HER2 were examined. Recent reports indicate that amino acids 309 and 310 on exon 8 are prone to mutations (G309A/E, S310F; refs. 24 and 47), a site that has previously not been identified to contribute to the HER2–Affibody interaction (44). As expected, no point mutations occurred in the outlier samples. Higher tissue efflux kinetics (k_2) paired with a lowered K_1 are indicative of lack of retention or potential perfusion deficits, causing reduced tracer delivery. If perfusion deficits are responsible for this unexpected finding, then an adverse implication on correct assessment of HER2 positivity by this technology is envisaged; the comparable clinical scenario is, however, unlikely to affect treatment stratification, as poor perfusion would potentially also reduce efficacy of trastuzumab.

Finally, we confirmed that [^{18}F]GE-226 is suitable as pharmacodynamic marker of HSP90 inhibition and perhaps as patient enrichment tool for those likely to benefit from such therapies. The most promising of these drugs, NVP-AUY922 (48) is currently in phase II clinical trials and has previously shown to downregulate HER2 expression (49), which was correctly confirmed *in vitro* and *in vivo* by [^{18}F]GE-226 PET. This is in accordance with the report by Smith-Jones and colleagues who similarly demonstrated that the HSP90 inhibitor, 17-allylaminogeldanamycin, degrades HER2 leading to reduction in the uptake of [^{68}Ga]-labeled F(ab′)$_2$ fragment of trastuzumab (43, 50).

In conclusion, [^{18}F]GE-226 PET imaging permits accurate discrimination of HER2 receptor expression, irrespective of tumor heterogeneity, cell lineage, or prior trastuzumab treatment. We expect the tracer to have good safety and dosimetry profiles because of its low nonspecific binding, the use of short-lived radiolabel and its favorable pharmacokinetic properties. These data support the clinical development of this tracer in patients with cancer, which is planned.

Disclosure of Potential Conflicts of Interest

P. Iveson has commercial research grant from GE Healthcare. P. Iveson also has ownership interest (including patents) in GE Healthcare. No potential conflicts of interest were disclosed by the other authors.

Authors' Contributions

Conception and design: S. Trousil, S. Hoppmann, P. Iveson, D. Hiscock, E.O. Aboagye
Development of methodology: S. Trousil, S. Hoppmann, P. Iveson, D. Hiscock, E.O. Aboagye
Acquisition of data (provided animals, acquired and managed patients, provided facilities, etc.): S. Trousil, S. Hoppmann, Q.D. Nguyen, M. Kaliszczak, P. Iveson, D. Hiscock
Analysis and interpretation of data (e.g., statistical analysis, biostatistics, computational analysis): S. Trousil, S. Hoppmann, G. Tomasi, E.O. Aboagye
Writing, review, and/or revision of the manuscript: S. Trousil, S. Hoppmann, Q.D. Nguyen, P. Iveson, D. Hiscock, E.O. Aboagye
Study supervision: D. Hiscock, E.O. Aboagye

Acknowledgments

The authors thank M. Glaser and B. Forrest for supporting radiochemistry, and M. Jones for sequencing support.

Grant Support

This work was supported by Cancer Research UK—Engineering and Physical Sciences Research Council grant (in association with the Medical Research Council and Department of Health, England) grant C2536/A10337.

The costs of publication of this article were defrayed in part by the payment of page charges. This article must therefore be hereby marked *advertisement* in accordance with 18 U.S.C. Section 1734 solely to indicate this fact.

Received September 9, 2013; revised December 9, 2013; accepted December 31, 2013; published OnlineFirst February 3, 2014.

References

1. Harari D, Yarden Y. Molecular mechanisms underlying ErbB2/HER2 action in breast cancer. Oncogene 2000;19:6102–14.
2. Carlsson J, Nordgren H, Sjostrom J, Wester K, Villman K, Bengtsson NO, et al. HER2 expression in breast cancer primary tumours and corresponding metastases. Original data and literature review. Br J Cancer 2004;90:2344–8.
3. Gravalos C, Jimeno A. HER2 in gastric cancer: a new prognostic factor and a novel therapeutic target. Ann Oncol 2008;19:1523–9.

4. Tai W, Mahato R, Cheng K. The role of HER2 in cancer therapy and targeted drug delivery. J Controlled Release 2010;146:264–75.
5. Ross JS, Fletcher JA. The HER-2/neu oncogene in breast cancer: prognostic factor, predictive factor, and target for therapy. Stem Cells 1998;16:413–28.
6. Hudis CA. Trastuzumab—mechanism of action and use in clinical practice. New Engl J Med 2007;357:39–51.
7. Olayioye MA, Neve RM, Lane HA, Hynes NE. The ErbB signaling network: receptor heterodimerization in development and cancer. EMBO J 2000;19:3159–67.
8. Zagozdzon R, Gallagher WM, Crown J. Truncated HER2: implications for HER2-targeted therapeutics. Drug Discov Today 2011;16:810–6.
9. Mohsin SK, Weiss HL, Gutierrez MC, Chamness GC, Schiff R, DiGiovanna MP, et al. Neoadjuvant trastuzumab induces apoptosis in primary breast cancers. J Clin Oncol 2005;23:2460–8.
10. Harris LN, You F, Schnitt SJ, Witkiewicz A, Lu X, Sgroi D, et al. Predictors of resistance to preoperative trastuzumab and vinorelbine for HER2-positive early breast cancer. Clin Cancer Res 2007;13: 1198–207.
11. Fabi A, Di Benedetto A, Metro G, Perracchio L, Nisticò C, Di Filippo F, et al. HER2 protein and gene variation between primary and metastatic breast cancer: significance and impact on patient care. Clin Cancer Res 2011;17:2055–64.
12. Shafi H, Astvatsaturyan K, Chung F, Mirocha J, Schmidt M, Bose S. Clinicopathological significance of HER2/neu genetic heterogeneity in HER2/neu non-amplified invasive breast carcinomas and its concurrent axillary metastasis. J Clin Pathol 2013;66:649–54.
13. Pauletti G, Godolphin W, Press MF, Slamon DJ. Detection and quantitation of HER-2/neu gene amplification in human breast cancer archival material using fluorescence in situ hybridization. Oncogene 1996;13:63–72.
14. Leyland-Jones B, Smith BR. Serum HER2 testing in patients with HER2-positive breast cancer: the death knell tolls. Lancet Oncol 2011;12:286–95.
15. Nygren P-Å. Alternative binding proteins: Affibody binding proteins developed from a small three-helix bundle scaffold. FEBS J 2008;275: 2668–76.
16. Löfblom J, Feldwisch J, Tolmachev V, Carlsson J, Ståhl S, Frejd FY. Affibody molecules: engineered proteins for therapeutic, diagnostic and biotechnological applications. FEBS Lett 2010;584:2670–80.
17. Tolmachev V, Orlova A, Nilsson FY, Feldwisch J, Wennborg A, Abrahmsen L. Affibody molecules: potential for *in vivo* imaging of molecular targets for cancer therapy. Expert Opin Biol Ther 2007;7: 555–68.
18. Glaser M, Iveson P, Hoppmann S, Indrevoll B, Wilson A, Arukwe J, et al. Three methods for 18F labeling of the HER2-binding affibody molecule ZHER2:2891 including preclinical assessment. J Nucl Med 2013;54: 1981–8.
19. Scaltriti M, Rojo F, Ocana A, Anido J, Guzman M, Cortes J, et al. Expression of p95HER2, a truncated form of the HER2 receptor, and response to anti-HER2 therapies in breast cancer. J Natl Cancer Inst 2007;99:628–38.
20. Workman P, Aboagye EO, Chung Y-L, Griffiths JR, Hart R, Leach MO, et al. Minimally invasive pharmacokinetic and pharmacodynamic technologies in hypothesis-testing clinical trials of innovative therapies. J Natl Cancer Inst 2006;98:580–98.
21. Zhao L, Ashek A, Wang L, Fang W, Dabral S, Dubois O, et al. Heterogeneity in lung 18FDG uptake in pulmonary arterial hypertension: potential of dynamic 18FDG positron emission tomography with kinetic analysis as a bridging biomarker for pulmonary vascular remodeling targeted treatments. Circulation 2013;128:1214–24.
22. Tomasi G, Bertoldo A, Bishu S, Unterman A, Smith CB, Schmidt KC. Voxel-based estimation of kinetic model parameters of the L-[1-(11)C]leucine PET method for determination of regional rates of cerebral protein synthesis: validation and comparison with region-of-interest-based methods. J Cereb Blood Flow Metab 2009;29: 1317–31.
23. Calderwood SK, Khaleque MA, Sawyer DB, Ciocca DR. Heat shock proteins in cancer: chaperones of tumorigenesis. Trends Biochem Sci 2006;31:164–72.
24. Bose R, Kavuri SM, Searleman AC, Shen W, Shen D, Koboldt DC, et al. Activating HER2 mutations in HER2 gene amplification negative breast cancer. Cancer Discov 2013;3:224–37.
25. Kramer-Marek G, Kiesewetter DO, Martiniova L, Jagoda E, Lee SB, Capala J. [18F]FBEM-Z(HER2:342)-Affibody molecule-a new molecular tracer for *in vivo* monitoring of HER2 expression by positron emission tomography. Eur J Nucl Med Mol Imaging 2008;35:1008–18.
26. Kramer-Marek G, Kiesewetter DO, Capala J. Changes in HER2 expression in breast cancer xenografts after therapy can be quantified using PET and 18F-labeled affibody molecules. J Nucl Med 2009;50:1131–9.
27. Kramer-Marek G, Gijsen M, Kiesewetter DO, Bennett R, Roxanis I, Zielinski R, et al. Potential of PET to predict the response to trastuzumab treatment in an ErbB2-positive human xenograft tumor model. J Nucl Med 2012;53:629–37.
28. Kramer-Marek G, Bernardo M, Kiesewetter DO, Bagci U, Kuban M, Aras O, et al. PET of HER2-positive pulmonary metastases with 18F-ZHER2:342 affibody in a murine model of breast cancer: comparison with 18F-FDG. J Nucl Med 2012;53:939–46.
29. Malmberg J, Sandstrom M, Wester K, Tolmachev V, Orlova A. Comparative biodistribution of imaging agents for in vivo molecular profiling of disseminated prostate cancer in mice bearing prostate cancer xenografts: focus on 111In- and 125I-labeled anti-HER2 humanized monoclonal trastuzumab and ABY-025 affibody. Nucl Med Biol 2011;38:1093–102.
30. Orlova A, Magnusson M, Eriksson TL, Nilsson M, Larsson B, Hoiden-Guthenberg I, et al. Tumor imaging using a picomolar affinity HER2 binding affibody molecule. Cancer Res 2006;66:4339–48.
31. Tolmachev V, Nilsson FY, Widstrom C, Andersson K, Rosik D, Gedda L, et al. In-111-benzyl-DTPA-Z(HER2:342), an affibody-based conjugate for *in vivo* imaging of HER2 expression in malignant tumors. J Nucl Med 2006;47:846–53.
32. Feldwisch J, Tolmachev V, Lendel C, Herne N, Sjoberg A, Larsson B, et al. Design of an optimized scaffold for affibody molecules. J Mol Biol 2010;398:232–47.
33. EudraLex. Volume 4 Good manufacturing practice (GMP) Guidelines. Brussels: European Commission; 2013 [cited 2013 Oct 9]. Available from: http://ec.europa.eu/health/documents/eudralex/vol-4/.
34. Ahlgren S, Orlova A, Wallberg H, Hansson M, Sandstrom M, Lewsley R, et al. Targeting of HER2-expressing tumors using 111In-ABY-025, a second-generation affibody molecule with a fundamentally reengineered scaffold. J Nucl Med 2010;51:1131–8.
35. Malmberg J, Perols A, Varasteh Z, Altai M, Braun A, Sandstrom M, et al. Comparative evaluation of synthetic anti-HER2 Affibody molecules site-specifically labelled with 111In using N-terminal DOTA, NOTA and NODAGA chelators in mice bearing prostate cancer xenografts. Eur J Nucl Med Mol Imaging 2012;39:481–92.
36. Xavier C, Vaneycken I, D'Huyvetter M, Heemskerk J, Keyaerts M, Vincke C, et al. Synthesis, preclinical validation, dosimetry, and toxicity of 68Ga-NOTA-anti-HER2 nanobodies for iPET imaging of HER2 receptor expression in cancer. J Nucl Med 2013;54:776–84.
37. Behr TM, Goldenberg DM, Becker W. Reducing the renal uptake of radiolabeled antibody fragments and peptides for diagnosis and therapy: present status, future prospects and limitations. Eur J Nucl Med 1998;25:201–12.
38. Orlova A, Tolmachev V, Pehrson R, Lindborg M, Tran T, Sandström M, et al. Synthetic affibody molecules: a novel class of affinity ligands for molecular imaging of HER2-expressing malignant tumors. Cancer Res 2007;67:2178–86.
39. Hoppmann S, Miao Z, Liu S, Liu H, Ren G, Bao A, et al. Radiolabeled affibody-albumin bioconjugates for HER2-positive cancer targeting. Bioconj Chem 2011;22:413–21.
40. Orlova A, Jonsson A, Rosik D, Lundqvist H, Lindborg M, Abrahmsen L, et al. Site-specific radiometal labeling and improved biodistribution using ABY-027, a novel HER2-targeting affibody molecule-albumin-binding domain fusion protein. J Nucl Med 2013;54:961–8.
41. Hofström C, Altai M, Honarvar H, Strand J, Malmberg J, Hosseinimehr SJ, et al. HAHAHA, HEHEHE, HIHIHI, or HKHKHK: influence of position and composition of histidine containing tags on biodistribution of [99mTc(CO)3]+-labeled affibody molecules. J Med Chem 2013;56: 4966–74.

42. Baum RP, Prasad V, Müller D, Schuchardt C, Orlova A, Wennborg A, et al. Molecular imaging of HER2-expressing malignant tumors in breast cancer patients using synthetic 111In- or 68Ga-labeled affibody molecules. J Nucl Med 2010;51:892–7.
43. Smith-Jones PM, Solit DB, Akhurst T, Afroze F, Rosen N, Larson SM. Imaging the pharmacodynamics of HER2 degradation in response to Hsp90 inhibitors. Nat Biotech 2004;22:701–6.
44. Eigenbrot C, Ultsch M, Dubnovitsky A, Abrahmsén L, Härd T. Structural basis for high-affinity HER2 receptor binding by an engineered protein. Proc Natl Acad Sci U S A 2010;107:15039–44.
45. Shukla R, Thomas TP, Peters JL, Desai AM, Kukowska-Latallo J, Patri AK, et al. HER2 specific tumor targeting with dendrimer conjugated anti-HER2 mAb. Bioconj Chem 2006;17:1109–15.
46. Valabrega G, Montemurro F, Aglietta M. Trastuzumab: mechanism of action, resistance and future perspectives in HER2-overexpressing breast cancer. Ann Oncol 2007;18:977–84.
47. Greulich H, Kaplan B, Mertins P, Chen TH, Tanaka KE, Yun CH, et al. Functional analysis of receptor tyrosine kinase mutations in lung cancer identifies oncogenic extracellular domain mutations of ERBB2. Proc Natl Acad Sci U S A 2012;109:14476–81.
48. Eccles SA, Massey A, Raynaud FI, Sharp SY, Box G, Valenti M, et al. NVP-AUY922: a novel heat shock protein 90 inhibitor active against xenograft tumor growth, angiogenesis, and metastasis. Cancer Res 2008;68:2850–60.
49. Oude Munnink TH, Korte MAd, Nagengast WB, Timmer-Bosscha H, Schröder CP, Jong JRd, et al. 89Zr-trastuzumab PET visualises HER2 downregulation by the HSP90 inhibitor NVP-AUY922 in a human tumour xenograft. Eur J Cancer 2010; 46:678–84.
50. Smith-Jones PM, Solit D, Afroze F, Rosen N, Larson SM. Early tumor response to Hsp90 therapy using HER2 PET: comparison with 18F-FDG PET. J Nucl Med 2006;47:793–6.